



Modelling a torrential event in a river confluence

M. Roca^a, J.P. Martín-Vide^{a,*}, P.J.M. Moreta^b

^a Universitat Politècnica de Catalunya, Department of Civil Engineering, Jordi Girona 1-3, D1, 08034 Barcelona, Spain

^b Hydraulics Consultant, IAHR Member, San Gerardo, 6, 3-1, 28035 Madrid, Spain

ARTICLE INFO

Article history:

Received 6 December 2007

Received in revised form 30 June 2008

Accepted 29 October 2008

Keywords:

River confluence

Torrential river

Two-dimensional modelling

Field data

SUMMARY

Torrential floods characterized by extremely high discharges and sediment transport rates are common in Mediterranean areas. Few field data is available for such floods due to sudden increase in water discharges and short flood duration. This paper presents the field data collected during a major flood event in a 90° confluence of two torrential rivers of the Mediterranean area. A two-dimensional model was used to describe the flow characteristics at the confluence. The influence on water levels of the torrential character of both rivers and some morphological processes as the tributary mouth gravel bar has been assessed. Although channel roughness coefficients and sediment deposits influence final water surface elevations they have lesser effect than the discharge ratio between main and tributary rivers.

© 2008 Elsevier B.V. All rights reserved.

Introduction

Torrential floods, common in Mediterranean areas, are characterized by extremely high discharges in comparison to mean annual flows and very high sediment transport rates. Flash floods in torrential ephemeral rivers (Martín-Vide et al., 1999) are the main natural hazard in northeastern Spain. In ungauged catchments, historical flood data and geomorphological studies may provide valuable information that can be used to prevent flooding (Rico et al., 2001). This paper presents an analysis of the hydraulics and flood processes at the junction of two rivers with an approximate confluence angle of 90°. These streams are considered torrential rivers as they have slopes steeper than 1.5% (Meunier, 1991) and exhibit high transport rates of both suspension and bed load during flood events.

Dynamics of open-channel flow at river confluences are dependent on channel geometry and flow parameters such as cross-section area, slope, angle of river junction, discharge ratio, downstream Froude number and hydraulic roughness. In torrential rivers, new parameters related to sediment characteristics should be added when sediment transport rates becomes important.

A large number of laboratory studies describing flow dynamics at confluences, some of them based on field data, can be found in the literature (Best and Reid, 1984; Ramamurthy et al., 1998; Biron et al., 1996, 2002; Weber et al., 2001; De Serres et al., 1999). In a 90° open-channel confluence zones of separation, stagnation and mixing are the main flow characteristics (Fig. 1). The zone of sep-

aration, created downstream of the junction, is characterized by lower water depths and flow velocities. Recirculation flow and upstream velocities can also be observed. Dimensions of this zone depend on discharge ratio, $Q_{main}/Q_{tributary}$, between main and tributary channels: higher ratios produce smaller areas (Gurram et al., 1997). The separation zone promotes flow contraction and higher main flow velocity at the main stem of the river. The stagnation zone located at the apex of the junction (upper corner) is also an area with low velocity (Weber et al., 2001) (Fig. 1). A shear plane with higher water depths develops from this point separating the main and tributary flows. The location of this mixing zone controls the spatial distribution of bedload transport rates and the associated morphological changes (De Serres et al., 1999).

Pronounced local scour at the confluence is a characteristic morphological process particularly when channel bed elevation between the main and tributary rivers is similar. However, in most natural channel junctions bed elevations of both rivers are discordant, hence the confluence morphology is transformed in a tributary mouth bar that ends as an avalanche face (De Serres et al., 1999). The presence of this “positive step” in the tributary, instead of a local scour hole, produces lateral fluid motion from the deeper main channel towards the shallower tributary, which generates higher turbulence levels. Fluctuations of the discharge ratio between the main and tributary channels causes the migration of the avalanche face at the confluence: as the main flow becomes dominant the avalanche face recedes from the junction. Another common morphological feature is the presence of a confluence bar just downstream of the junction in the separation zone.

Two-dimensional flow models that take into account the flow in the main and transverse directions have been widely used in the

* Corresponding author. Tel.: +34 93 401 64 76; fax: +34 93 401 73 57.

E-mail addresses: martaroca4@gmail.com (M. Roca), vide@grahi.upc.edu (J.P. Martín-Vide), pmarmor@ciccp.es (P.J.M. Moreta).

Nomenclature

A	cross-sectional area (m^2)	t	time
A_{basin}	total basin area	u	velocity in x -direction
C	Chézy coefficient	U	depth-averaged velocity component in x -direction
c_f	dimensionless bottom shear stress coefficient	U'	shear velocity in x -direction
c_μ	dimensionless eddy viscosity coefficient	V	depth-averaged velocity component in y -direction
D_{50}	median grain size diameter (m)	x	downstream reference coordinate
g	acceleration due to gravity	y	transverse reference coordinate
H	depth of water above the bed level	z_b	bed elevation
K	constant with length dimensions	$\beta_{uu}, \beta_{uv}, \beta_{vu}, \beta_{vv}$	Boussinesq coefficients
n	manning coefficient	κ	von Karman's constant
Q_m	mean annual discharge	ρ	density of water
Q_{500}	water discharge for the 500-year return period	ν	depth-averaged directional eddy viscosity
Q_{main}	main water discharge, Francolí river (m^3/s)	ν_o	constant value of kinematic eddy viscosity
Q_{Total}	total water discharge downstream of the junction (m^3/s)	τ_{xb}, τ_{yb}	bottom shear stresses in the x - and y -directions, respectively
$Q_{\text{tributary}}$	tributary water discharge, Brugent river (m^3/s)	$\tau_{xx}, \tau_{xy}, \tau_{yx}, \tau_{yy}$	shear stresses caused by turbulence
S	bed slope		

last decade thanks to the technical development in computing allowing to run large and complex simulations. Examples of different hydraulic models for studying complex river flow configurations can be found in the literature: River2D (Vasquez, 2005), TRIMR2D (Denlinger et al., 2002), FESWMS-2DH (Martín-Vide et al., 2002; Zanichelli et al., 2004), TELEMAC-2D (Asaro and Paris, 2000). Duan and Nanda (2006) and Weerakon et al. (2003) have validated 2D models with laboratory data in confluences demonstrating the applicability of the classic Navier–Stokes depth-averaged equations to these river configurations. Mathematical models of river confluences must take into account the bed morphology because it has a significant effect on the flow characteristics (De Serres et al., 1999).

This paper presents field data collected during a major flood event that is used to qualitatively describe the flow evolution and morphological features at the confluence. A two-dimensional flow analysis is performed with the numerical model FESWMS-2DH in order to describe quantitatively the flow field. The paper also presents a simple methodology based on field data to take into account the torrential character of both rivers in the 2D analysis.

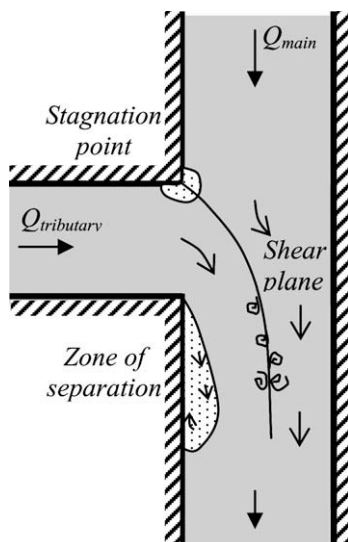


Figure 1. Flow diagram at a 90° river confluence.

Site description

The studied site is at the junction of the Francolí and Brugent rivers in La Riba, in the Mediterranean area of northeastern Spain (Fig. 2). La Riba, with a large textile and paper industrial tradition, has several old constructions close to the river channel that used to rely on the Francolí river water power for their operations.

Upstream of the confluence the main river Francolí flows around a sharp bend in a narrow mountain pass composed of conglomerate, chalky and dolomitic rocks. The tributary river Brugent joins at the right side of the main river at an approximate angle of 90°. During flood events the main channel of the tributary flows through a large fan of gravel material built up at the confluence.

There are five bridges around the confluence. A railway and a road bridge cross the Francolí river in the upstream part of the reach (Fig. 2) but they do not influence either its main channel or its floodplain. There are two more bridges over the Francolí, one of which is an arch bridge (at the bottom of the map in Figs. 2 and 3 right), and another crossing the Brugent river. These three bridges have a far more significant impact on the hydraulics and river morphology of the study reach.

Table 1 shows the main characteristics of the rivers at the confluence.

The alluvial bed material in the main river (Francolí) is armored with $D_{50} = 60$ mm at the surface and $D_{50} = 7.4$ mm below it. The tributary bed material is coarser and contains some boulders, around one meter size, from nearby terraces. In addition, vegetation grows up at the confluence during long periods of low discharge.

Field data in the case study

On 10th October 1994, during the rainy season in the Mediterranean area, a major flood event that lasted 24 h caused severe damage throughout the Francolí basin. Close to the confluence of the Brugent and the Francolí in La Riba, the bridge over the Brugent river was destroyed, whereas the arch bridge over the Francolí was overtopped and partially damaged (Fig. 3, right). Some buildings directly opposite to the confluence were also damaged (an old mill was completely destroyed) and several surrounding buildings were flooded (Fig. 3, left). Various types of field data were collected, including rainfall data, maximum water level marks, the thickness of sediment deposits, eyewitness accounts and video recordings.

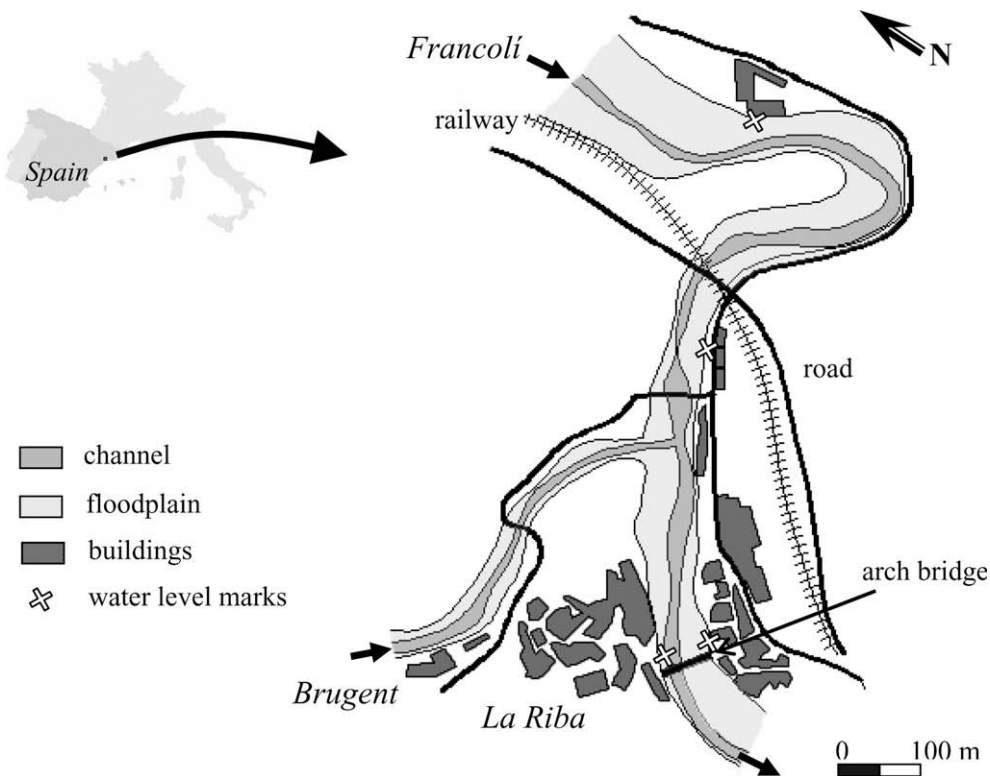


Figure 2. Sketch of the confluence of the Francolí and Brugent rivers in La Riba.

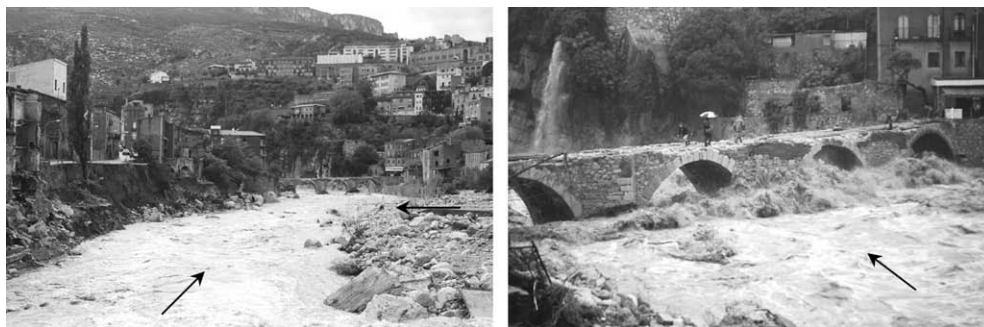


Figure 3. (left) Downstream view of the Francolí river: building damages on the left bank and deposits of material from the Brugent on the right (arrows indicate flow direction of the Francolí, from bottom to top, and the Brugent, from right to left); (right) Arch bridge over the Francolí river downstream of the junction, shortly after peak discharge.

The maximum flood discharge in the tributary river was estimated from rainfall data by using hydrological models. In addition, water surface levels from the area of the fallen bridge were incorporated into a one-dimensional model to obtain a hydraulic estimate of the maximum discharge. The peak value obtained for the tributary river in both methods was approximately $600 \text{ m}^3/\text{s}$.

The peak value for the main river was also estimated from rainfall-runoff and water surface elevation data. In this case, water level marks were obtained from a bed-rock cross-section upstream of the confluence (uppermost high water level mark in Fig. 2). The channel at this point was narrower due to the nat-

ural topography of the canyon and the presence of a mill. Therefore, this section was under critical flow conditions so there was a unique relationship between water level and discharge. The flow rate obtained was around $800 \text{ m}^3/\text{s}$. The sum of the Francolí and Brugent discharge downstream of the arch bridge was estimated about $1100 \text{ m}^3/\text{s}$ by using water level marks and hydrological approximations.

Sediment transport data was obtained from the upstream reach of the main river. The peak flow carrying suspended load entered the basement of the mill through a window acting as a suspended sediment trap during the flood (Fig. 4). The water level rose to 1.6 m. Once the floodwater had receded, the sediment load settled down and accumulated forming a 40-cm-thick layer of mud. The concentration of suspended material calculated from this data was approximately 25%. This value can be extrapolated to the tributary river, where the sediment concentration may have been even higher due to the large volume of available material in the basin (Pujadas, 1994).

Table 1
Main channel characteristics of the Francolí and Brugent rivers.

	A_{basin} (km ²)	S (%)	Q_m (m ³ /s)	Q_{500} (m ³ /s)
Francolí	838	1.7	1.23	1600
Brugent	69	2.9	0.44	520

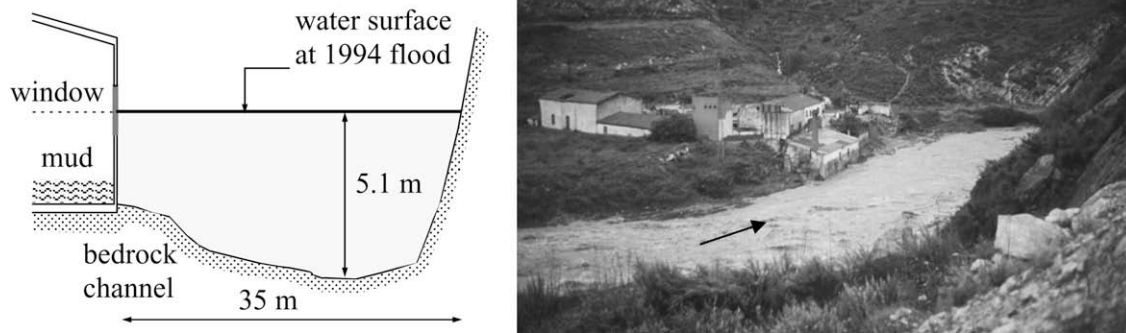


Figure 4. Cross-section of the canyon and downstream view of the area during the flood.

Flood level marks were recorded in the confluence area on both banks of the arch bridge and in some buildings on the left bank of the Francolí river, just upstream of the second bridge (Fig. 2). The marks are separated by a distance of 300 m and the water level difference is approximately 3.5 m, so the water surface slope was 1%. These marks were used to validate the numerical results.

Another old mill located in a straight, uniform reach of the Francolí river 20 km downstream of the confluence had also recorded the marks of several flood events from the 20th Century, including the 1994 flood (Fig. 5). The water levels and maximum discharges estimated at this site were used to assess the torrential character of the flood.

Field data enabled us to describe the evolution of the 1994 flood at the confluence. The Brugent, which is the tributary river, was the first to rise during the early morning October 10th. At 8 a.m. the bridge over the tributary collapsed due to overtopping: this is the reference time for the Brugent peak discharge. From field data and eyewitness accounts it was determined that the worst damage at the confluence was caused by the flooding of the tributary river. Meanwhile, the discharge in the Francolí river was still low so the tributary significantly blocked the flow of the main river. This is observed in some videotapes recorded during the flood event and inferred from the presence of floating debris moving steadily in the upstream canyon. The main river reached its peak discharge at 11 a.m.

At 6 p.m., 10 h after the peak discharge in the Brugent river was recorded, the water surface levels in the main river had lowered and sediment deposition became visible at the confluence. The

avalanche face of the tributary bar contained material of different grain size including boulders of one meter size in the bar front (Fig. 6a). The tributary bar was extended several meters upstream and had a sediment thickness of up to 2 m in some sections. Gravel deposits filled the tributary channel and forced the river to open into two channels, as can be seen in Fig. 6a. An extensive downstream junction bar is also shown in Figure 6b. During the rising phase of the main river hydrograph the tributary mouth bar was probably partially flushed away (Fig. 3 left).

The presence of boulders in the bar downstream of the junction and in the middle of the main river channel is also shown by a photograph taken after a major flood in 1930 (Fig. 6c). This material came from the tributary river and may have been too large to be removed by the main river flow.

Description of the numerical model

The FESWMS-2DH numerical model was used to study the flow at the confluence during the 1994 flood. It has been developed by the US Federal Highway Administration (FHWA, 2002) based on the vertically-averaged momentum conservation equations in the main and transverse flow directions and the continuity equation. The equations of this depth-averaged, shallow water model are written as follows:

Continuity equation:

$$\frac{\partial H}{\partial t} + \frac{\partial(HU)}{\partial x} + \frac{\partial(HV)}{\partial y} \quad (1)$$

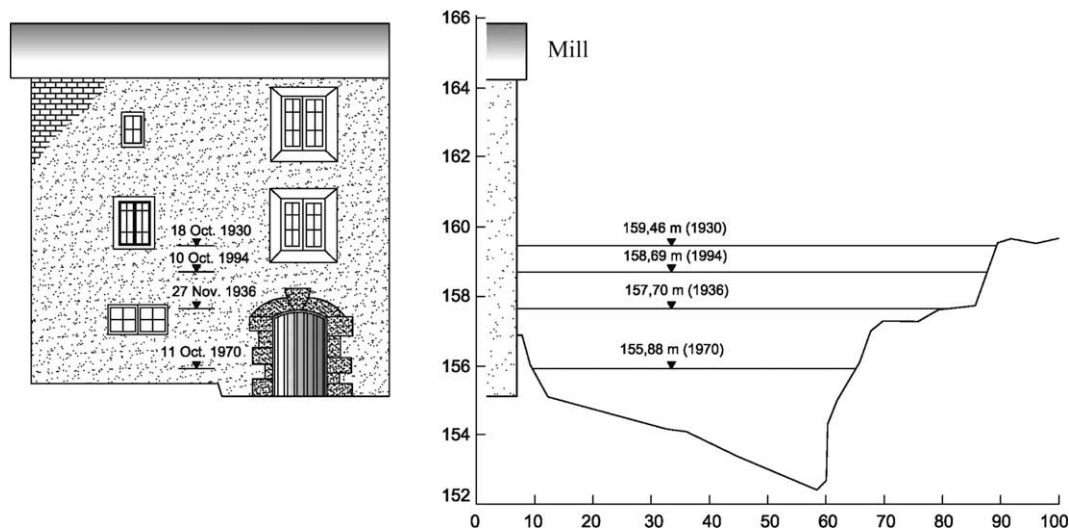


Figure 5. Sketch of flood marks at the mill located 20 km downstream of the confluence; front view (left) and cross-section of the Francolí river at the mill (right).

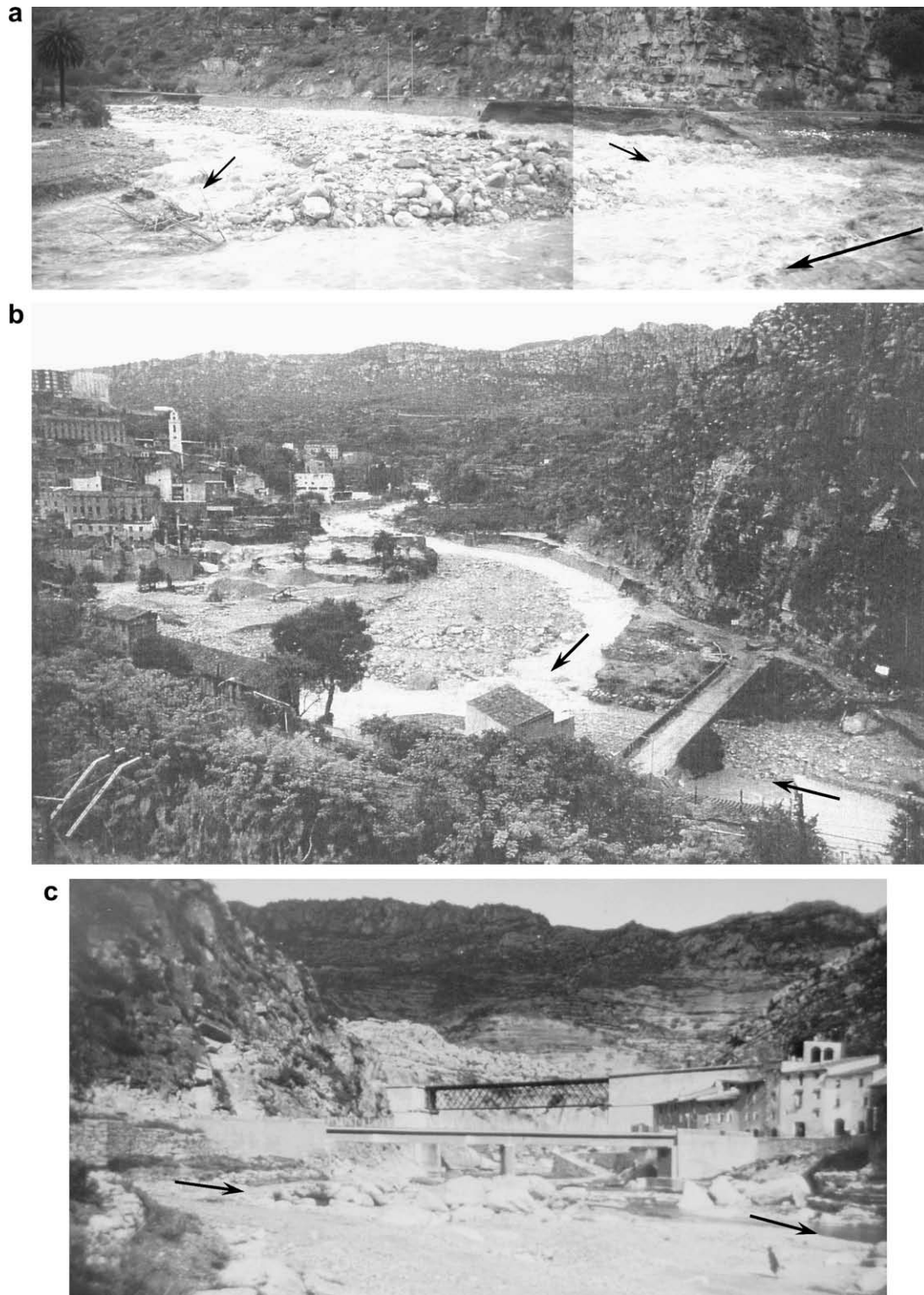


Figure 6. (a) Detail of the front bar of the Brugent river on the evening of October 10th 1994. The large arrow indicates the flow direction of the Francolí. Two channels over the tributary mouth bar were opened by the Brugent (two small arrows); (b) general view of the confluence the day after the flood event; the Francolí river flows from right to left and the Brugent river from top to bottom; (c) upstream view from right bank of the Francolí after the 1930 flood. Arrows indicate flow direction of the Brugent (left) and the Francolí (right); the small bridge just upstream of the confluence is the same as in (b).

Momentum equation in x :

$$\frac{\partial(HU)}{\partial t} + \frac{\partial(\beta_{uu}HU^2)}{\partial x} + \frac{\partial(\beta_{uv}HUV)}{\partial y} + \frac{1}{2}g\frac{\partial H^2}{\partial x} + gH\frac{\partial z_b}{\partial x} + \frac{1}{\rho}\left[\tau_{xb} - \frac{\partial(H\tau_{xx})}{\partial x} - \frac{\partial(H\tau_{xy})}{\partial y}\right] = 0 \quad (2a)$$

Momentum equation in y :

$$\frac{\partial(HV)}{\partial t} + \frac{\partial(\beta_{vu}HUV)}{\partial x} + \frac{\partial(\beta_{vv}HV^2)}{\partial y} + \frac{1}{2}g\frac{\partial H^2}{\partial y} + gH\frac{\partial z_b}{\partial y} + \frac{1}{\rho}\left[\tau_{yb} - \frac{\partial(H\tau_{yx})}{\partial x} - \frac{\partial(H\tau_{yy})}{\partial y}\right] = 0 \quad (2b)$$

where H is the depth, U and V are the vertically-averaged velocities in the x and y -directions, $\beta_{uu}, \beta_{uv}, \beta_{vu}, \beta_{vv}$ are the Boussinesq coefficients that take into account the variation of velocity in the vertical, z_b is the bed elevation, τ_{xb} and τ_{yb} are bottom shear stresses in the x and y -directions, respectively, $\tau_{xx}, \tau_{xy}, \tau_{yx}, \tau_{yy}$ are the shear stresses caused by turbulence, ρ is the water density and g is gravity.

In FESWMS, the vertical distribution of the main velocity is calculated as

$$u = \frac{U_*}{\kappa} \log\left(\frac{z - z_b}{K}\right) \tag{3}$$

where $U_* = \sqrt{c_f} U$ is the bed shear velocity, κ is von Karman's constant, K is a constant with length dimensions and c_f is a dimensionless bottom shear stress coefficient that can be calculated by using the Manning roughness (n) or the Chézy (C) coefficients as

$$c_f = \frac{gn^2}{H^{1/3}} = \frac{g}{C^2} \tag{4}$$

The bottom shear stresses are expressed as

$$\tau_{xb} = \rho c_f U (U^2 + V^2)^{1/2} \left[1 + \left(\frac{\partial z_b}{\partial x}\right)^2 + \left(\frac{\partial z_b}{\partial y}\right)^2 \right]^{1/2} \tag{5}$$

$$\tau_{yb} = \rho c_f V (U^2 + V^2)^{1/2} \left[1 + \left(\frac{\partial z_b}{\partial x}\right)^2 + \left(\frac{\partial z_b}{\partial y}\right)^2 \right]^{1/2} \tag{6}$$

Boussinesq's eddy viscosity concept is used to express the depth-averaged stresses caused by turbulence:

$$\tau_{xx} = \rho \nu 2 \frac{\partial U}{\partial x} \tag{7a}$$

$$\tau_{yx} = \rho \nu \left(\frac{\partial U}{\partial y} + \frac{\partial V}{\partial x} \right) \tag{7b}$$

$$\tau_{yy} = \rho \nu 2 \frac{\partial V}{\partial y} \tag{7c}$$

where ν is the depth-averaged directional eddy viscosity. In FESWMS the eddy viscosity is isotropic so $\nu = \nu_{xx} = \nu_{xy} = \nu_{yx} = \nu_{yy}$, which is expressed as

$$\nu = \nu_0 + c_\mu U_* H \tag{8}$$

where ν_0 is a constant value of kinematic eddy viscosity and c_μ is a dimensionless coefficient. The FESWMS Manual (FHWA, 2002) suggested a value $c_\mu = 0.6$ for natural rivers. Radojkovic and Djordjevic (1985) obtained good approximations with values of c_μ between 0.25 and 0.65. Martín-Moreta (2003) used a value of $1.0 \text{ m}^2/\text{s}$ for the constant kinematic eddy viscosity (ν_0) obtaining good agreement with laboratory data. FESWMS has been successfully used to assess problems in divergences as junctions (Zanichelli et al., 2004) or flow around islands (Martín-Moreta, 2003).

Model application

The confluence area modeled was large enough to correctly simulate the influence at the boundaries (Fig. 7). The simulation mesh of the study area contained 3500 elements, most of which were triangular. The mesh was based on a digital elevation model (LIDAR data) with known coordinates (x,y,z) at intervals of 1 m. The main river flow distribution at the entrance to the calculation mesh is only affected by the downstream reach, with no influence of the upstream sharp bend. The downstream boundary was set at the arch bridge where it was possible to determine water levels from flood marks. The tributary river area was also large enough to capture all of the significant phenomena that occurred at the confluence.

In order to simulate the flow at a confluence using the FESWMS-2DH numerical model it is necessary to establish discharges of the

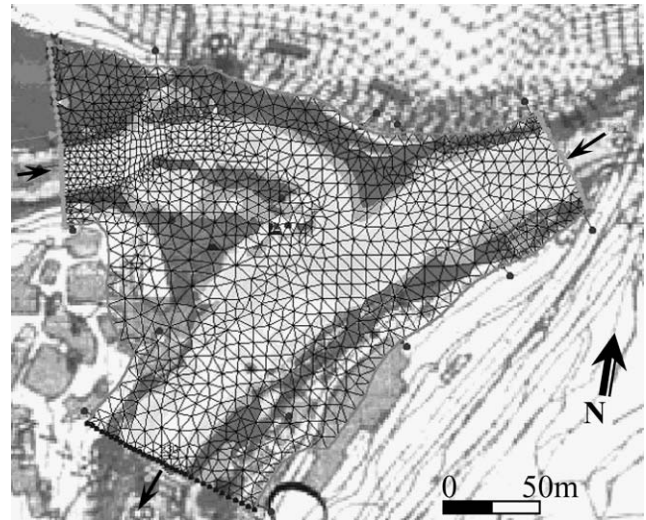


Figure 7. Mesh of the study area used in the 2D hydraulic model.

main and tributary rivers and surface level at the downstream cross-section (boundary condition). Several discharge combinations for the main and tributary rivers were studied in order to simulate the 1994 flood. Only the most relevant values are presented in this paper (Table 2). The total discharge downstream of the confluence was set at $1100 \text{ m}^3/\text{s}$ in all runs, which is the maximum possible value downstream of the arch bridge based on the evidence of flood marks. Run R1 was considered to be the most realistic discharge combination for at least the early morning of the studied flood event, as we used values of $600 \text{ m}^3/\text{s}$ for the tributary and $500 \text{ m}^3/\text{s}$ for the main river. To verify the influence of the discharge ratio $Q_{main}/Q_{tributary}$ the opposite situation, i.e. a larger peak discharge for the main river, was also studied (Run R2), A water discharge of $700 \text{ m}^3/\text{s}$ for the tributary river, although unrealistic, was useful to describe the situation in which the tributary river blocked the main river flow (Run R3).

Table 2
Water discharge combinations.

Run	Q_{main}	$Q_{tributary}$	Q_{total}	$Q_{main}/Q_{tributary}$
R1	500	600	1100	0.83
R2	700	400	1100	1.75
R3	400	700	1100	0.57

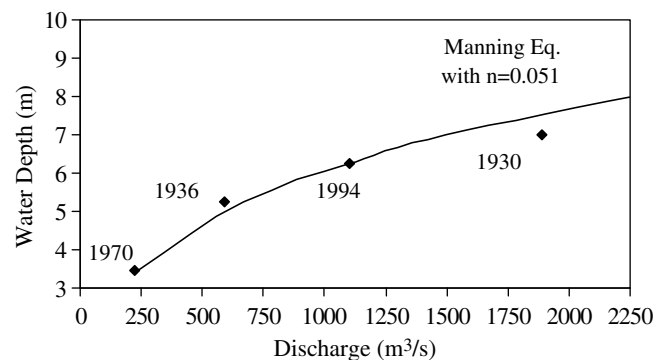


Figure 8. Water depth versus discharge in several historical floods (dates plotted) at the mill (in Fig. 5). Manning equation using 0.051 as roughness coefficient is plotted.

Water level marks at the arch bridge were used as downstream boundary condition and were kept constant during all runs shown in Table 2. The eddy viscosity was set at each element in the mesh by using Eq. (8) and assuming $\nu_0 = 1.0 \text{ m}^2/\text{s}$ and $c_\mu = 0.5$ for all of the study cases.

A roughness coefficient was assigned to every mesh element. We considered three possibilities according to the position of the element in the fluvial system: river channel, urban areas and vegetated banks and floodplains. The roughness coefficient n was set at 0.02 for urban areas, which include buildings considered as ineffective areas, whereas 0.06 was used for vegetated areas. The roughness coefficient for the river channel, where sediment transport takes place, should be sensitive to the torrential nature of the

floods in the Francolí and Brugent rivers. We therefore used the set of flood marks at the old mill located 20 km downstream of the confluence (Fig. 5) to take this into account (Helmbrecht and Martín-Vide, 2006). The Manning equation was used to link discharges and water levels recorded during previous floods at the mill (Fig. 8). This was the method used to derive the apparent n roughness coefficients, which are equivalent to the actual bulk friction in torrential flows. Part of this high friction is produced by the suspended load (Wan and Wang, 1994; Chien and Wan, 1999).

The best fit was obtained with a mean value $n = 0.051$ (Fig. 8), which is much larger than grain roughness coefficient associated with bed material (0.021). This value was assigned to the mesh elements located in the river channel. Values of n of 0.04 and 0.06

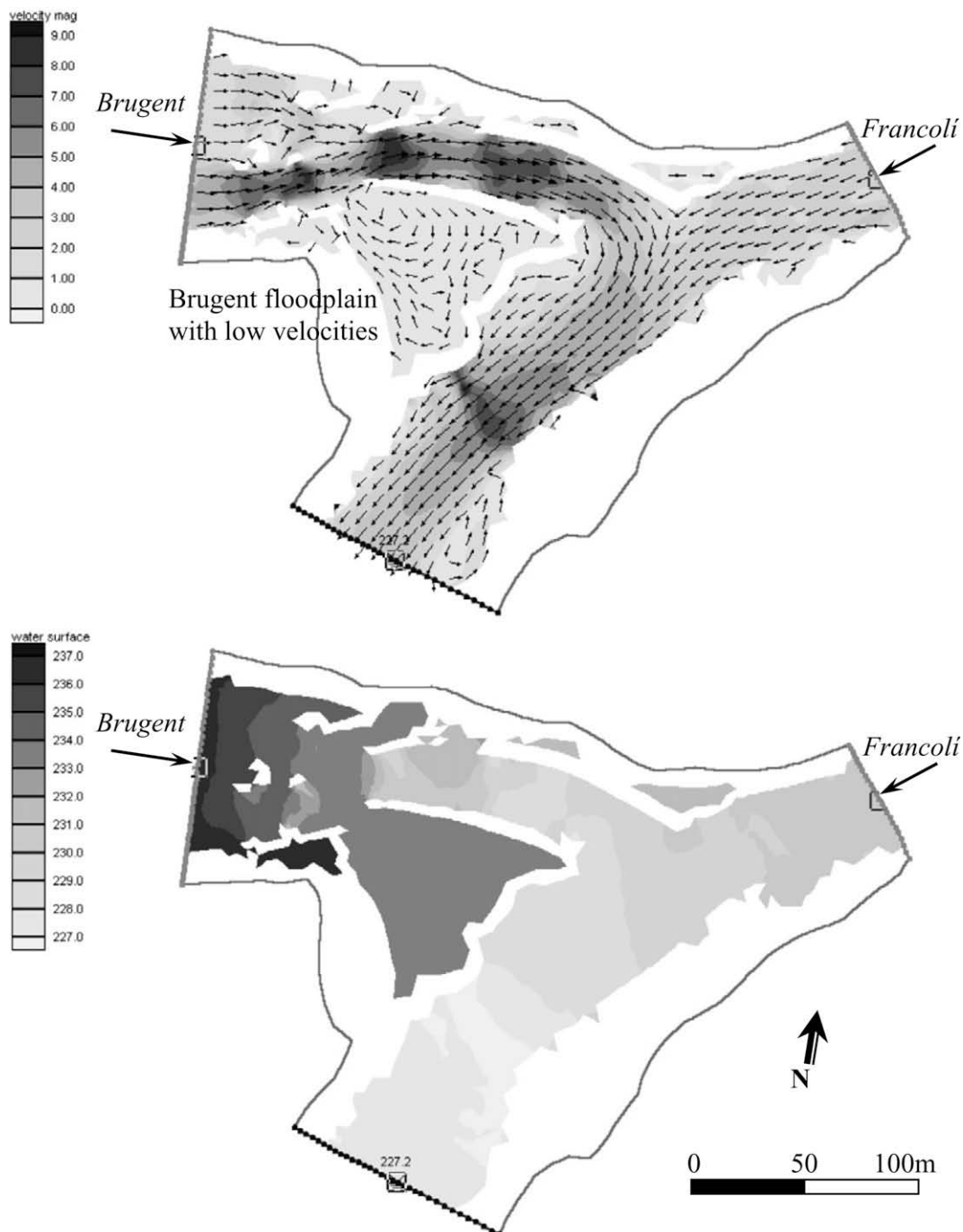


Figure 9. Velocity (top) and water surface (bottom) maps for run R1. Darker shading indicates higher values of the variable. Arrows show flow direction and not magnitude.

were also considered to assess the influence of roughness coefficients on the flow confluence.

Modelling results

The numerical results show that velocities of the tributary and main river upstream of the confluence decrease due to mixing of flows at the junction. Just downstream of the confluence the main river velocity increases at the left bank. A separation zone with low velocities develops at the right bank, adjacent to the area in which the tributary flow joins the main flow (Fig. 9). These numerical results can be qualitative compared with the field observations obtained from videotapes of the 1994 flood, showing a good agreement.

The tributary river flow shifts from subcritical to supercritical and vice versa reaching velocities up to 10 m/s. Water transversal slopes produced high levels close to the stagnation point. In the most realistic run, R1 water surface levels of the main river upstream of the confluence are quite constant as it is observed in the videotape recordings. Water levels increase at the left bank downstream of the confluence where higher velocities are also calculated (Fig. 9).

Fig. 10 shows the effect of the discharge ratio on the surface levels upstream of the confluence. The free surface profiles in the main river are higher in R3 than in R2, although the flow discharge in the main river is higher in R2 (700 m³/s) than in R3 (400 m³/s). Therefore, if the $Q_{main}/Q_{tributary}$ rate decreases we should conclude that the main river flow is blocked by the tributary. A jump in the water level 80 m upstream of the boundary condition is caused by a bed slope change and channel narrowing.

The influence of roughness coefficients on water levels clearly depends on water discharge ratio. The roughness effect is minimal upstream of the confluence when $Q_{main}/Q_{tributary}$ is low: water levels are primarily affected by the tributary flow. Water surface levels increase slightly at the confluence reach when roughness coefficient increases. Roughness has a greater influence when $Q_{main}/Q_{tributary}$ is higher: water levels rise throughout the main river reach, even upstream of the confluence.

Bed morphology is an important issue in the hydraulic modelling of any event. Unfortunately, bed changes through time as well as bank changes during the flood, especially those of the tributary mouth bar are not known. A run with the same hydraulic and roughness conditions as run R1 but with different bed geometry was considered. A prism-like block of between 0.1 and 1.5 m was added to increase the elevation of the initial bed topography at the avalanche face and along the channel bed of the Brugent river. These values and the geometry of the raised area were extracted from field data at the end of the flood event. The confluence bar defined in this way can be considered a discordance between the main and tributary river beds. Therefore, the energy losses increase in that area and water levels in the main river rise. In addition, the avalanche face decreases flow velocities of the main river upstream of the confluence.

Water level marks on the left bank of the main river upstream of the confluence were used to check the validity of the numerical results. A good agreement was obtained by comparing the field marks with results of run R1 in which $Q_{main} = 500$ m³/s, $Q_{tributary} = 600$ m³/s and a roughness coefficient of $n = 0.060$. The agreement between the calculated levels and field data improves when considering the simulation of the avalanche face (Fig. 11).

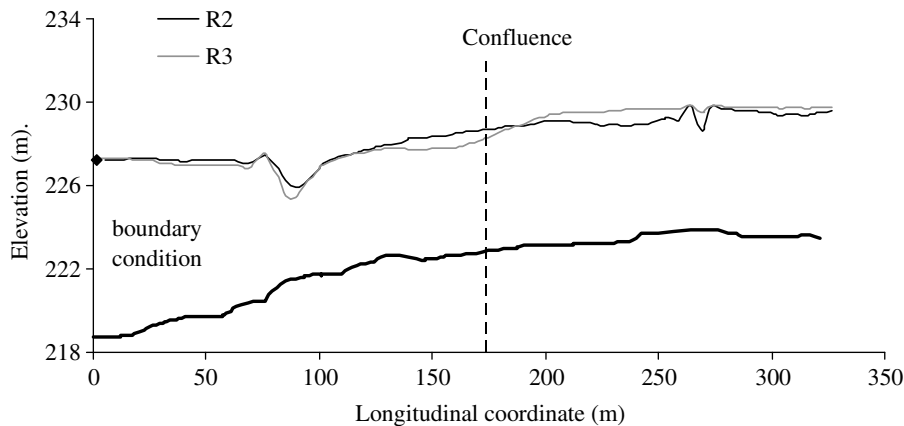


Figure 10. Water surface profiles in the Francoli river for runs R2 and R3.

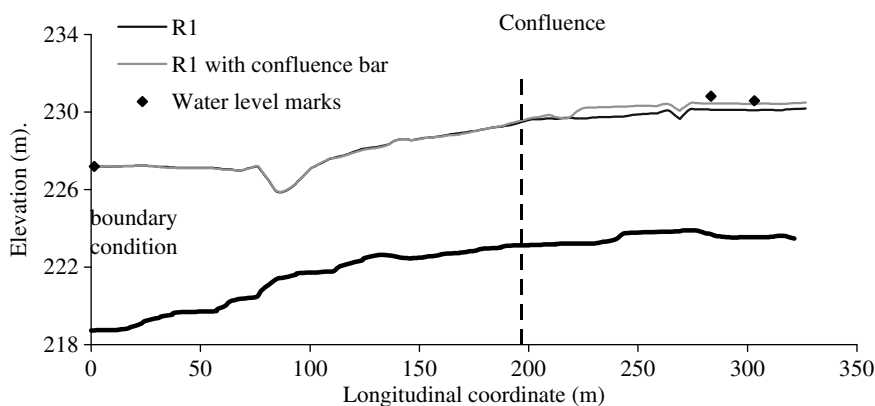


Figure 11. Water surface profiles in the Francoli river for run R1 modifying the channel geometry to include a confluence bar.

Discussion and conclusions

There is few field data on flood events in the Mediterranean rivers due to the flash-flood nature of the hydrographs and their high sediment load which makes difficult to record hydraulic parameters and geometry changes during the flooding, limiting the understanding of flow dynamics, processes and geomorphology. Therefore, even limited field data such as that for the 1994 flood of the Francolí and Brugent rivers are valuable.

The effects of torrential flow in the main and tributary rivers are considered by increasing the roughness coefficient of the channels from 0.021 to 0.051, where major sediment transport took place. This is a very simple methodology for numerical simulations. An “equivalent” roughness coefficient has been successfully applied to discharge–depth relationships in other torrential rivers in the Mediterranean area (Helmbrecht and Martín-Vide, 2006). Field data is required to obtain reasonable values of these equivalent coefficients.

Confluence bar morphology and its temporal variations depend on sediments transported by the tributary river and the role of the main flow sweeping deposits away during the flood. In the simulations done with FESWMS the river bed configuration at the end of the flood event has been used as a means of simplifying the problem. However, it seems to be a reasonable approximation as it shows fairly good agreement with field data.

Flow configuration at the confluence is mainly determined by the $Q_{main}/Q_{tributary}$ ratio. Channel roughness coefficients and sediment deposits also influence final water surface elevations but they have lesser effect than discharge ratio.

The results obtained with the 2D model for the 1994 flood give enough confidence to use FESWMS in the flood risk assessment of the Francolí river. Water levels at the confluence were obtained for different scenarios with the 2D model and linked with the results of the one-dimensional model applied to assess flood risk in the Francolí catchment. The 2D model uses as downstream boundary condition the levels obtained with the 1D model. Then, water levels obtained in the upstream sections of the main and tributary rivers were used as boundary conditions in the 1D model for river reaches further upstream of the confluence. The results obtained show that flooding is still possible in La Riba urban area despite recent training works on the left bank. The worst scenarios are related to peak discharge in the tributary river blocking the flow from the Francolí River.

Acknowledgment

The photographs in Figs. 3, 4 and 6a, c were obtained courtesy of Jordi Pujadas, whom the authors would also like to thank for his useful data and observations.

References

- Asaro, G., Paris, E., 2000. The effects induced by a new embankment at the confluence between two rivers: TELEMAC results compared with a physical model. *Hydrological Processes* 14, 2345–2353.
- Best, J.L., Reid, I., 1984. Separation zone at open-channel junctions. *Journal of Hydraulic Engineering* 110 (11), 1588–1594.
- Biron, P.M., Best, J.L., Roy, A.G., 1996. Effects of bed discordance on flow dynamics at open channel confluences. *Journal of Hydraulic Engineering* 112 (12), 676–682.
- Biron, P.M., Richer, A., Kirkbride, A.D., Roy, A.G., Han, S., 2002. Spatial patterns of water surface topography at a river confluence. *Earth Surface Processes and Landforms* 27, 913–928.
- Chien, N., Wan, Z., 1999. *Mechanics of Sediment Transport*. ASCE Press.
- De Serres, B., Roy, A.G., Biron, P.M., Best, J.L., 1999. Three-dimensional structure of flow at a confluence of river channels with discordant beds. *Geomorphology* 26, 31–335.
- Denlinger, R.P., O’Connell, D.R.H., House, P.K., 2002. Robust determination of stage and discharge: an example from an extreme flood on the Verde river, Arizona. Ancient floods, modern hazards: principles and application of paleoflood hydrology. *Water Science and Application* 5, 127–146.
- Duan, J.G., Nanda, S.K., 2006. Two dimensional depth averaged model simulation of suspended sediment concentration distribution in a groyne field. *Journal of Hydrology* 327, 426–437.
- Federal Highway Administration (FHWA), 2002. User’s manual for FESWMS Flo2DH. Two-dimensional depth-averaged flow and sediment model. Publication no. FHWA-RD-03-053.
- Gurram, S.K., Karki, K.S., Hager, W.H., 1997. Subcritical junction flow. *Journal of Hydraulic Engineering* 123 (5).
- Helmbrecht, J., Martín-Vide, J.P., 2006. Principles and examples of torrential flow computation. *Ingeniería Civil* 141, 137–141 (in Spanish).
- Martín-Moreta, P., 2003. 2D model for vegetated rivers; calibration with Besòs river data. MS Thesis, UCLM, Ciudad Real, Spain (in Spanish).
- Martín-Vide, J.P., Niñerola, D., Bateman, A., Navarro, A., Velasco, E., 1999. Runoff and sediment transport in a torrential ephemeral stream of the Mediterranean coast. *Journal of Hydrology* 225 (3–4), 118–129.
- Martín-Vide, J.P., Martín-Moreta, P.J., López-Querol, S., Machado, M.J., Benito, G., 2002. Tagus river: historical floods at Talavera de la Reina. Palaeofloods, historical floods and climatic variability: applications in flood risk assessment. In: *Proc. PHEFRA Workshop*, Barcelona, October, pp. 191–196.
- Meunier, M., 1991. *Éléments d’hydraulique torrentielle*. Cemagref, Grenoble.
- Pujadas, J., 1994. Flood risk maps in the Francolí river at La Riba. Technical report for the Catalan Water Authority (Junta d’Aigües) (in Spanish).
- Radojkovic, M., Djordjevic, S., 1985. Computation of discharge distribution in compound channels. In: *Proc. 21st IAHR Congress*, Melbourne, vol. 3, pp. 367–371.
- Ramamurthy, A.S., Carballada, L.B., Tran, D.M., 1998. Combining open channel flow at right angled junctions. *Journal of Hydraulic Engineering* 114 (12), 1449–1460.
- Rico, M., Benito, G., Barnolas, A., 2001. Combined palaeoflood and rainfall–runoff assessment of mountain floods (Spanish Pyrenees). *Journal of Hydrology* 245, 59–72.
- Vasquez, J.A., 2005. Two-dimensional numerical simulation of flow diversions. In: *17th Canadian Hydrotechnical Conference*, Edmonton, Alberta, August 17–19.
- Wan, Z., Wang, Z., 1994. Hyperconcentrated Flow. *IAHR Monograph*. A.A.Balkema, Rotterdam.
- Weber, L.J., Schumate, E.D., Mawer, N., 2001. Experiment on flow at a 90° open-channel junction. *Journal of Hydraulic Engineering* 127 (5), 340–350.
- Weerakon, S.B., Tamai, N., Kawahara, Y., 2003. Depth averaged flow computation at a river confluence. *Proceedings of the Institution of Civil Engineers–Water Maritime and Energy*, London 156 (1), 73–83.
- Zanichelli, G., Caroni, E., Fiorotto, V., 2004. River bifurcation analysis by physical and numerical modeling. *Journal of Hydraulic Engineering* 130 (3), 237–242.